N95- 23618

NAVIER-STOKES FLOW FIELD ANALYSIS OF COMPRESSIBLE FLOW IN A PRESSURE RELIEF VALVE

Bruce Vu & Ten-See Wang
Computational Fluid Dynamics Branch
NASA - Marshall Space Flight Center

Ming-Hsin Shih & Bharat Soni
Engineering Research Center for Computational Field Simulation
Mississippi State University

Abstract

The present study was motivated to analyze the complex flow field involving gaseous oxygen (GOX) flow in a relief valve (RV). The 9391 RV, pictured in Figure 1, was combined with the pilot valve to regulate the actuation pressure of the main valve system. During a high-pressure flow test at Marshall Space Flight Center (MSFC) the valve system developed a resonance chatter, which destroyed most of the valve body. Figures 2-4 show the valve body before and after accident. It was understood that the subject RV has never been operated at 5500 psia. In order to fully understand the flow behavior in the RV, a computational fluid dynamics (CFD) analysis is carried out to investigate the side load across the piston sleeve and the erosion patterns resulting from flow distribution around piston/nozzle interface.

Grid Topology

The safety RV consists of a main cylinder and a piston, with a smaller diameter inlet. An intersection technique was developed to model the piston-cylinder configureation (Figure 5). To simplify the geometry, the diameter of the cylinder is kept constant.

An O-type grid in the axial plane was initially considered for this geometry. However, it would become very difficult to generate grid lines around the piston on the upper part of the main cylinder, if not impossible. H-type grid was then chosen to model this internal flow geometry. The main cylinder was cut into half at the plane of symmetry to reduce the size of domain. It was again cut into halves at the bottom face of the piston to divide the computational domain into upper part and lower part. To model the field geometry, the descritization was carried out into five-block zonal grid; the inlet itself formed a block, the lower part of the main cylinder formed another block, and the upper part of the main cylinder was cut into 3 more blocks. The 5-block grid is shown in Figures 6-7. Compared to the original O-type grid, this H-type grid topology greatly reduced the grid distortion, especially near the piston .

Grid Generation

GENIE++ (Ref. 1-3), a general purpose three-dimensional grid generation package, was used to generate the grid for this geometry. GENIE++ is the Mississippi State University updated version of INGRID (Ref. 4-5) developed by Arnold Engineering Development Center (AEDC).

In order to perform the surface intersections of the piston, as well as the inlet, with the main cylinder, an intersection algorithm with Newton-Ralphson method was used to obtain the intersection curves. Weighted transfinite interpolation (Weighted TFI) (Ref. 2) algorithm is used to generate the algebraic grid. Weighted TFI can be formulated as uniform TFI with grid

distribution mesh, where the grid distribution mesh is obtained by performing uniform TFI on normalized arc length distribution on associated boundaries (or surfaces in volume grid).

Since the selected grid topology reduced the distortion of grid lines, the resulting algebraic grid was very satisfactory, and no elliptic smoothing was performed for the present computation. However, for future grid-dependent study, elliptic solver will be applied to refine the local grids while maintaining a packed, viscous grid on the surface.

Governing Equations and Computational Scheme

The present numerical simulation uses a non-staggered grid, pressure based transport equation solver with an extended version of two-equation k-ε turbulence model. While the computer code has all-speed capability for both compressible and incompressible flows, the present study only uses the compressible feature. The basic equations employed to describe the momentum and heat transfer in the computational domain are the three-dimensional Reynolds-averaged transport equations. To solve the system of coupled nonlinear partial differential equations, it uses finite difference approximations to establish a system of linearized algebraic equations. An adaptive upwinding scheme is utilized to model the convective terms of the momentum, energy and continuity equations, which is based on the second and fourth order central differencing with artificial dissipation. Discretization of viscous fluxes and source terms uses a second-order central difference approximation. For velocity-pressure coupling, the present solution procedure employs pressure-based, predictor followed by multi-corrector approach. Details of the present numerical methodology are given by Wang and Chen (Ref. 6).

Due to symmetry, the computational domain occupies only the front half of the RV. Along all solid walls, no-slip condition is applied for velocities, and temperature is assumed constant. For near-wall turbulence treatment, it uses a wall function with modified flux source and a velocity profile capable of providing a smooth transition between logarithmic law-of-wall and linear variation in viscous sublayer. Such a treatment significantly reduces the flux dependence on the near-wall spacing. The inlet conditions are fully developed profiles for velocities and turbulence parameters, and the outlet conditions satisfy the conservation of mass.

Result and Discussion

The preliminary computations have been performed to simulate the flow field of GOX in the 9391 RV at 5500 psia and 1000° R. Results indicated no viscous heating due to low temperature gradients near the piston surface (Figure 8). The surface pressure contours in Figure 9 also indicated an insignificant side load across the piston sleeve. The force obtained from integrating all pressure points around the piston surface, from the bottom up to the piston sleeve is found to be only 70 lbf, under this adverse condition. The velocity vectors, magnitude, and Mach contours are shown in Figures 10-12, respectively. Finally, the vortex formations in Figure 13-14 predicts reasonable erosion patterns in the gap between the cylinder elbow and the bottom of the piston. Evidently these patterns are in agreement with the damaged hardware which indicates clear signs of burns and scratches near the piston/throat region.

References

1. Soni, B.K., Thompson, J.F., Stokes, M., and Shih, M.H.,"GENIE++, EAGLEView, and TIGER: General and Special Purpose Graphically Interactive Grid Systems", AIAA-92-0071, AIAA 30th Aerospace Sciences Meeting and Exhibit, Reno, Nevada, 1992.

2. Soni, B.K., "Grid Generation for Internal Flow Configurations", Computers Math. Application, Vol. 24, No. 516, pp.191-201, 1992.

3. Soni, B.K., "Two and Three Dimensional Grid Generation for Internal Flow Application of Computational Fluid Dynamics", AIAA-85-1526, AIAA 7th Computational Fluid Dynamics Conference, Cincinnati, Ohio, 1985.

4. Soni, B.K., and Dorrell, E.W., "INGRID Interactive Geometry-Grid Generation for Two Dimensional Applications", AEDC-TR-86-49.

5. Dorrell, E.W., and McClure, M.D., "3D INGRID: Interactive Three-Dimensional Grid Generation", AEDC-TR-87-40.

6. Wang, T.S. and Chen, Y.S., "A Unified Navier-Stokes Flowfield and Performance Analysis of Liquid Rocket Engines," AIAA-90-2494, AIAA/SAE/ASME/ASEE 26th Joint Propulsion Conference, Orlando, FL, July 1990.

George C. Marshall Space Flight Center
Structures and Dynamics Laboratory
Computational Fluid Dynamics Branch

NASA

Navier-Stokes Flow Field Analysis of Compressible Flow in a Pressure Relief Valve

By

B.T. Vu & T.S. Wang
Marshall Space Flight Center

M.H. Shih & B.K. Soni
Mississippi State University
Enginering Research Center

For

Workshop for CFD Applications in Rocket Propulsion
April 20-22, 1993
Huntsville, Alabama

NASA

BACKGROUND

TS116 Mishap Investigation:

- Mishap occured at X-15 while 40K test system was supposed to be in static state.
- The pressure relief valves have never been operated at 5500 psi.
- There are no data except valve activation times, personnel observations, and remaining parts of the subject relief valve.

NASA

OBJECTIVE

To investigate the following action items:

- Friction due to hot GOX flow across nozzle/piston interface
- Side load on piston sleeve
- Velocities at valve inlet nozzle
- Erosion patterns caused by vortex formations

NASA

APPROACH

- 1-D analytical solutions assuming convergent-divergent nozzle flow for initial flow field
- 3-D, multi-block, H-type grid generated by Genie++ using new intersection technique
- Numerical solutions by a pressure-based flow solver (FDNS-3D) assuming flow to be viscous, turbulent and compressible

NASA

RESULTS & DISCUSSION

- FDNS performs well on the coarse grids.
- F=70 lbf, based on 3-D analysis for the single-phase flow through a wide gap (0.16"). This side load results from integrating all pressure points (computed by FDNS) around the piston surface, from the bottom up to the piston sleeve.
- No viscous heating due to low temperature gradients.
- Low pressure drops across the piston indicate insignificant side loads.
- 3-D calculation indicates recirculation around piston/throat region.
- Vortex formation patterns agree with physical evidence from the damaged hardware.

NASA

SUMMARY

- Multi-block, 3-D, H-type grid was generated. Total of 91,612 grid points.
- Side loads calculated.
- Flow conditions provided to failure investigation team.
- Due to the complexity of grid and flow definition, 3-D problem becomes very expensive, e.g. the cost for a converged single-phase solution is recorded as:

1000 iterations = 9.5 cpu hours = 79.2 calendar hours

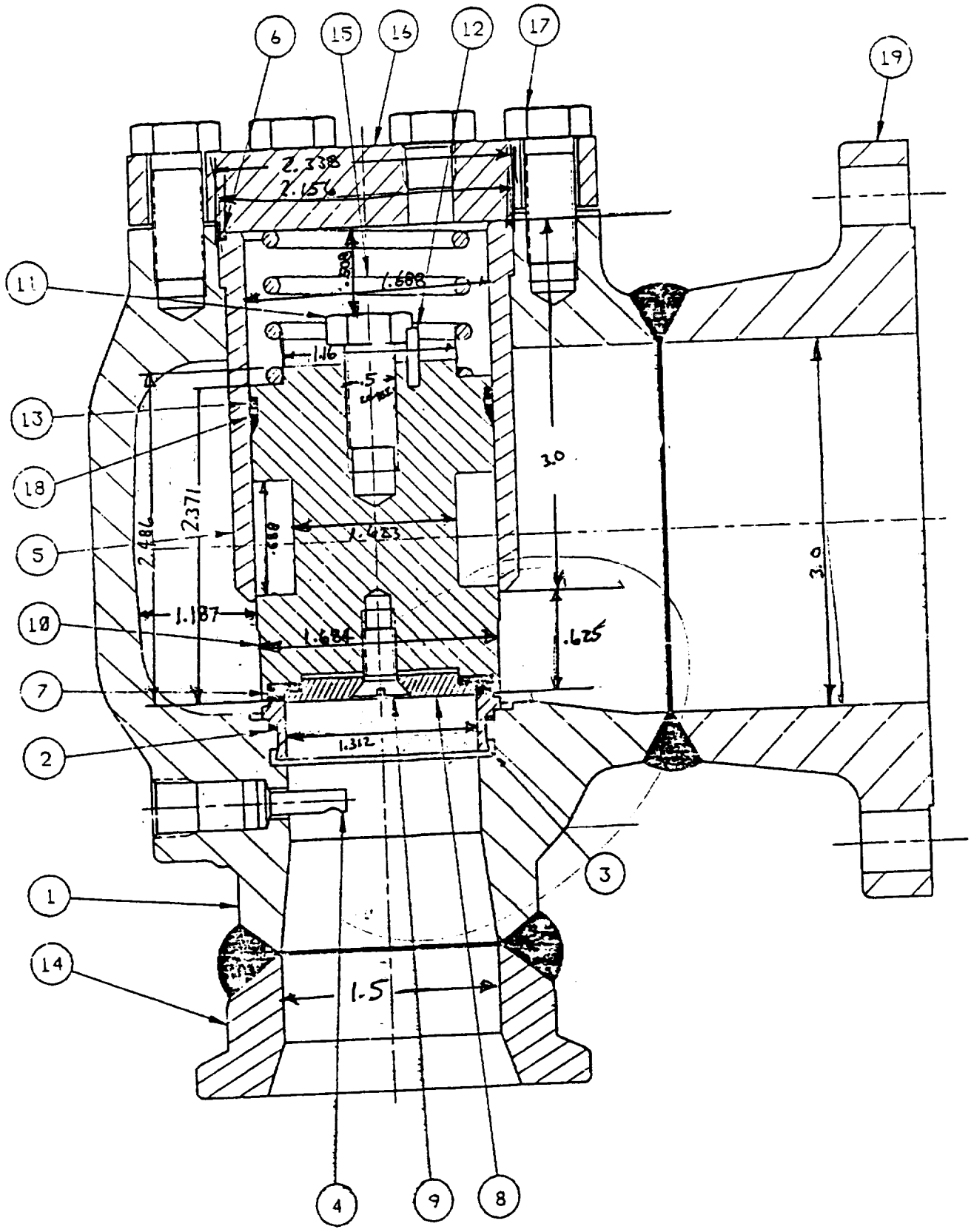

Figure 1. Valve schematic

Figure 2. Valve photo (before accident)

Figure 3. Side-view photo (after accident)

Figure 4. End-view photo (after accident)

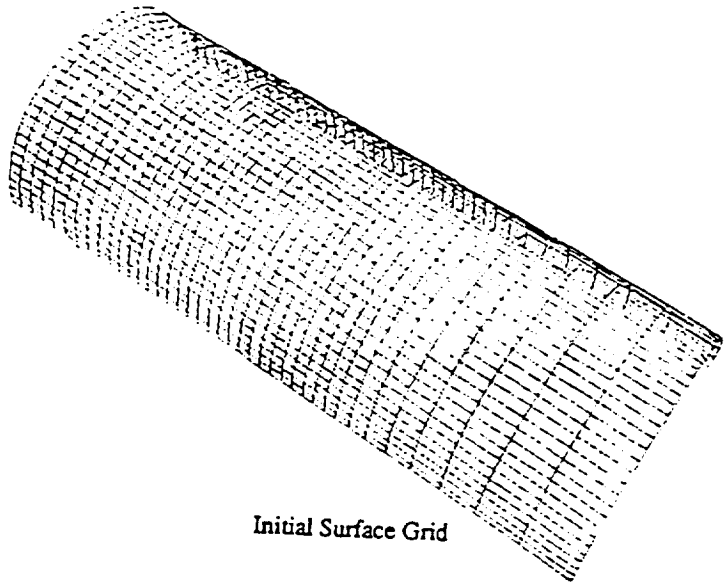

Initial Surface Grid

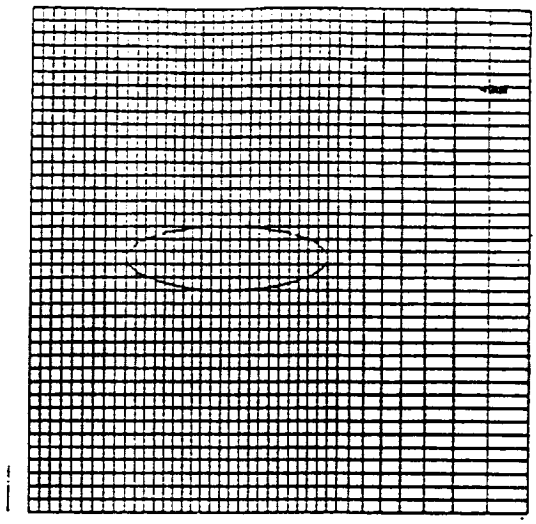

Parametric Values for Initial Surface and The Interior Object

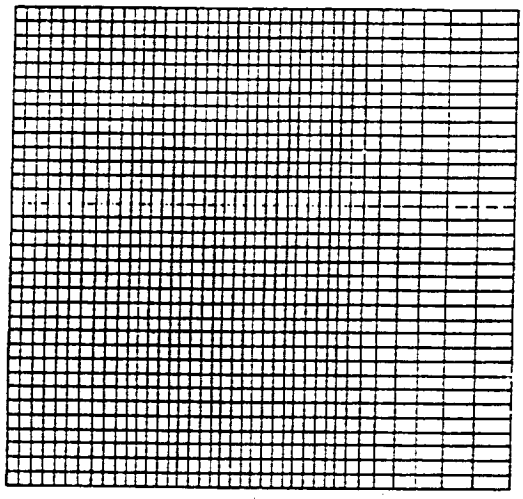

Parametric Space Associated with The Initial Surface Grid

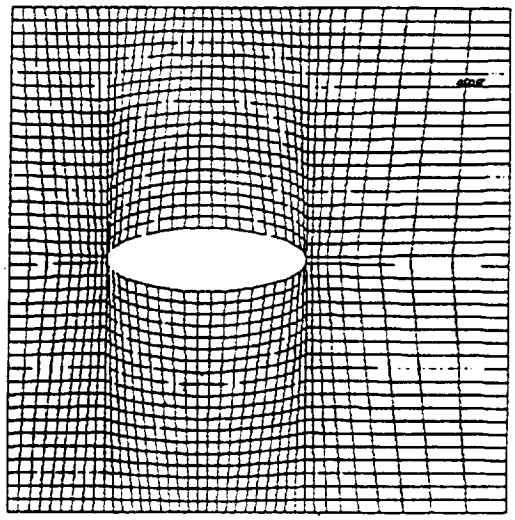

Reparameterized Distribution Space

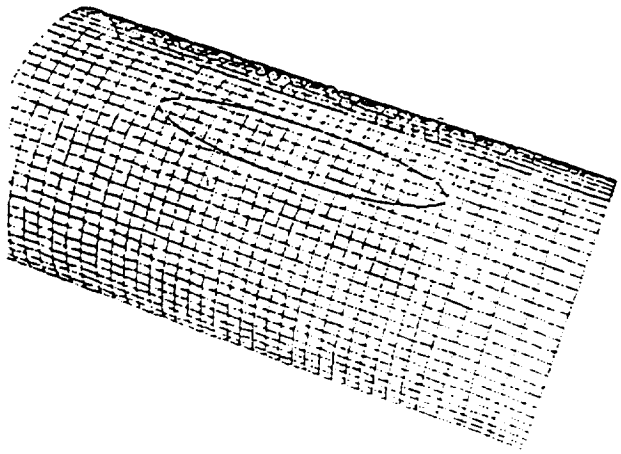

Interior Object on The Surface

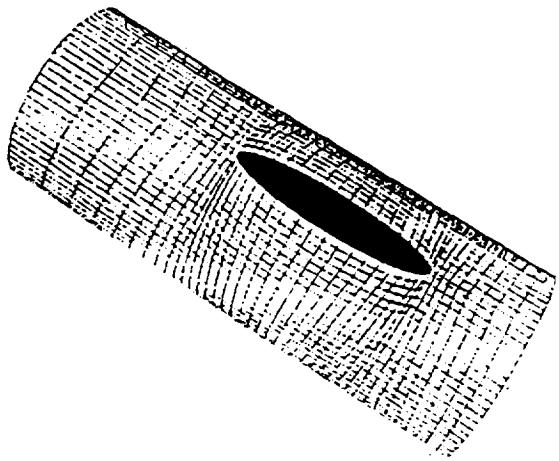

Resulting Surface Grid

Figure 5. Intersection technique

C-2

Figure 6. Three-dimensional grid (side-view)

Figure 7. Three-dimensional grid (end-view)

Figure 8. Temperature contours

Figure 9. Pressure contours

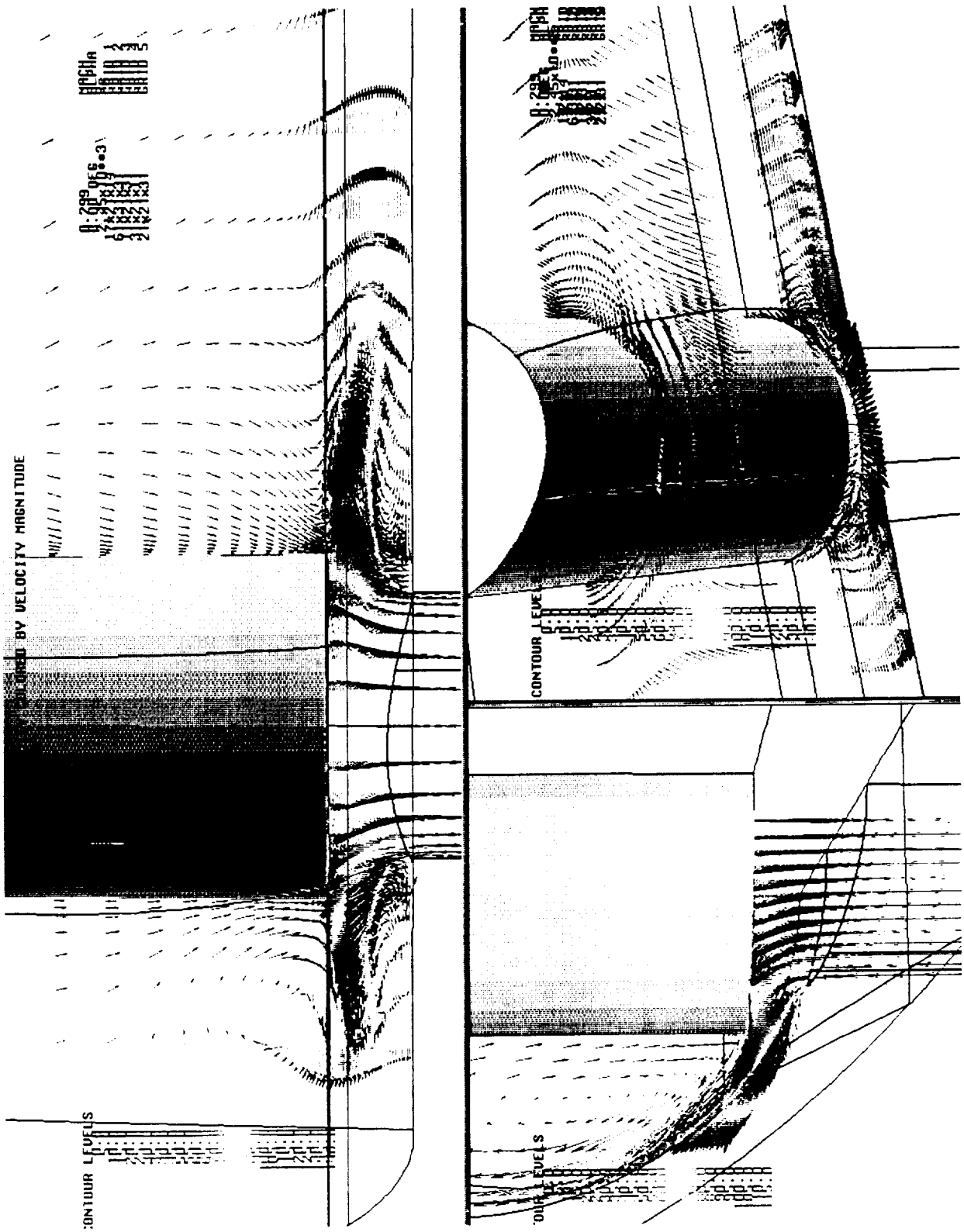

Figure 10. Velocity vectors

Figure 11. Velocity contours

Figure 12. Mach contours

Figure 13. Particle tracing

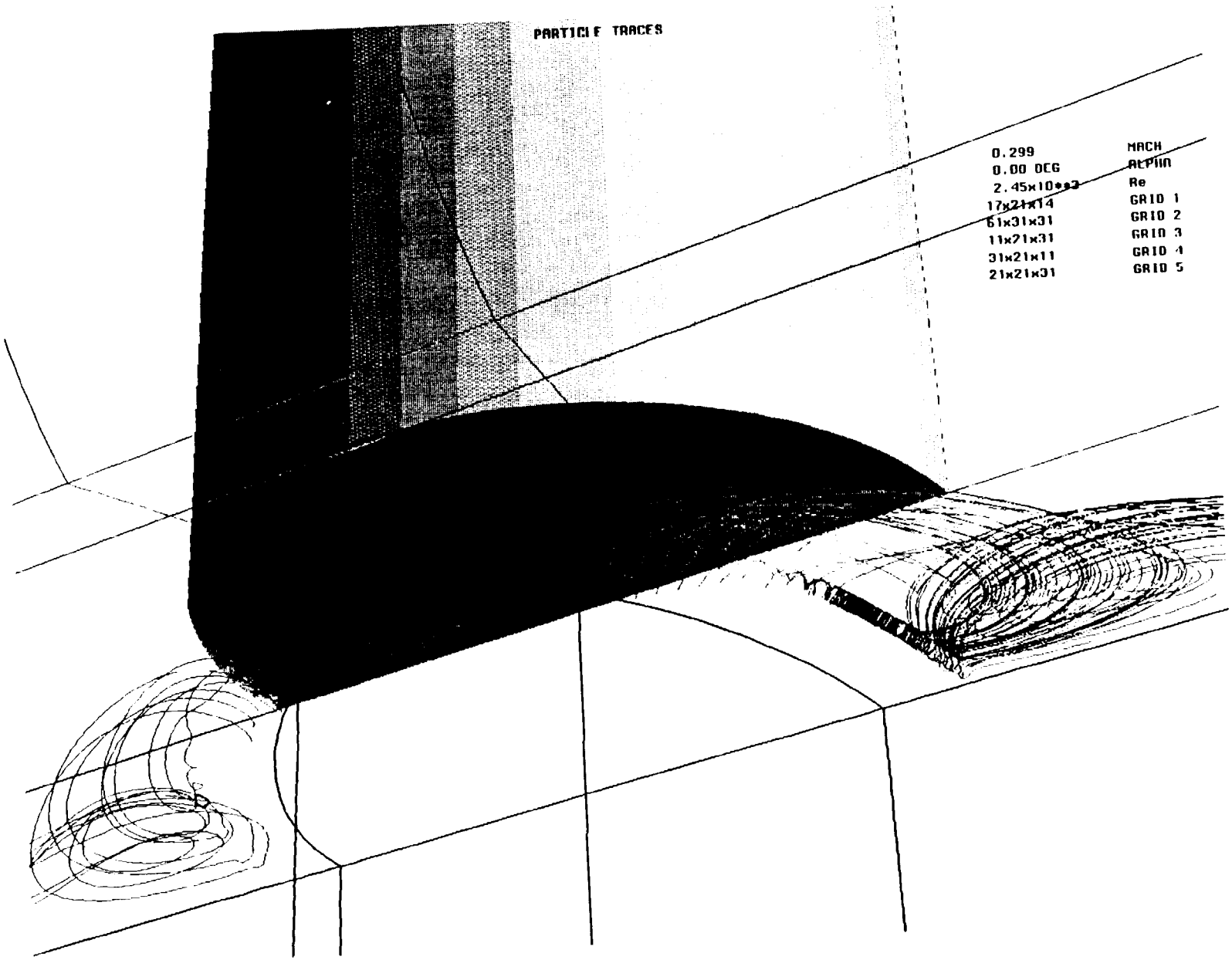

Figure 14. Particle tracing (close-up)